Catalysis Letters (2020) 150:482–492
https://doi.org/10.1007/s10562-019-03016-x

Unveiling the Structure Sensitivity for Direct Conversion of Syngas to C2-Oxygenates with a Multicomponent-Promoted Rh Catalyst

Xiaohui Sun[1] · Harrie Jansma[1] · Toshihito Miyama[2] · Rasika Dasanayake Sanjeewa Aluthge[2] · Kenichi Shinmei[2] · Noritoshi Yagihashi[2] · Haruka Nishiyama[2] · Dmitrii Osadchii[1] · Bart van der Linden[1] · Michiel Makkee[1]

Received: 29 August 2019 / Accepted: 21 October 2019 / Published online: 6 November 2019

Abstract

Mn and Li promoted Rh catalysts supported on SiO_2 with a thin TiO_2 layer were synthesized by stepwise incipient wetness impregnation approach. The thin TiO_2 layer on the surface of SiO_2 was proved to stabilize those small Rh nanoparticles and hinder their agglomeration. The reducibility of Rh on these catalysts depends on Rh particle size as well as the position of manganese oxide, and large Rh nanoparticles with MnO on Rh nanoparticles can be only reduced at an elevated temperature. Catalyst with large Rh particles exhibits a higher CO conversion and higher products selectivity towards long chain hydrocarbons and C2-oxygenates at the expense of decreasing methane formation than a similar catalyst with smaller Rh particles. This was attributed to the synergistic effect of Mn and Li promotion and molar ratio between Rh^0 and $Rh^{\delta+}$ sites on the surface of Rh nanoparticles. Moreover, Rh nanoparticles on MnO are proved to be more efficient in promoting hydrogenation of acetaldehyde to ethanol than its counterpart with MnO on Rh nanoparticles. Finally, in order to target high C2-oxygenates selectivity, low reaction temperature together with a low H_2/CO ratio in the feed is recommended.

Graphic Abstract

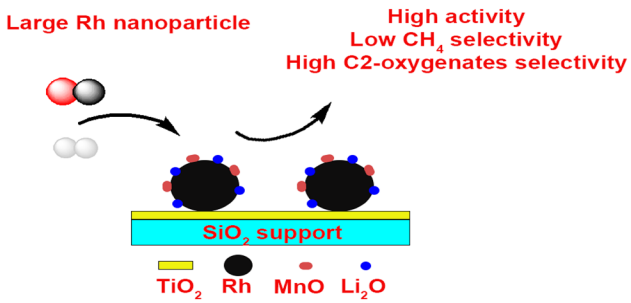

Keywords Ethanol · Acetaldehyde · Rh · Mn · Particle size

Electronic supplementary material The online version of this article (https://doi.org/10.1007/s10562-019-03016-x) contains supplementary material, which is available to authorized users.

✉ Xiaohui Sun

✉ Michiel Makkee
M.Makkee@tudelft.nl

[1] Catalysis Engineering, Department of Chemical Engineering, Delft University of Technology, Van der Maasweg 9, 2629 HZ Delft, The Netherlands

[2] Clean Technology & Advanced Materials Institute R&D Center, SEKISUI CHEMICAL CO., LTD., 32, Wadai, Tsukubashi, Ibaraki 300-4292, Japan

1 Introduction

The synthesis of renewable fuels such as ethanol has received extensive attention in recent years for its application both as a fuel additive and an energy carrier [1–3]. Nowadays, ethanol is produced mainly by fermentation of biomass-derived sugars [4]. Catalytic conversion of syngas (mixture of H_2 and CO obtained from natural gas, coal or biomass) to oxygenated compounds (ethanol, acetaldehyde and acetic acid), followed by a subsequent hydrogenation of acetaldehyde and acetic acid provides an alternative route

to produce ethanol at large scales. Several catalytic systems, including rhodium- and/or molybdenum sulfide-based catalysts, and modified Fischer–Tropsch and/or methanol synthesis catalysts have been studied for this purpose [5–8]. Slow kinetics and poor oxygenates selectivity in this process remain, however, the major obstacles. Hence, exploring catalysts with new structure and compositions for C2-oxygenates synthesis with high activities and oxygenated compounds selectivity still remains a big challenge.

Several transition metals in Group VIII of the Periodic Table have been investigated in CO hydrogenation, and products were found to clearly depend on the property of metals. Metals (e.g. Ir and Pd) that hardly dissociate CO, favor methanol production [9, 10], while cobalt and iron preferably produce long chain hydrocarbons owning to their high capability in CO dissociation [11–14]. Importantly, rhodium, that is located at an intermediate position in the periodic table, and possesses a unique CO adsorption behavior, has been proved highly efficient in the synthesis of C2-oxygenated compounds from CO hydrogenation [15–17]. Generally stating, CO hydrogenation to C2-oxygenates occurs on the surface of rhodium particles. Therefore, the number of active sites, namely the activity is a function of rhodium dispersion [15]. In order to achieve an uniform rhodium distribution, the intrinsic feature of supports and catalyst preparation conditions are supposed to be considered during a catalyst design [18–20]. For instance, silica with large surface area favors the dispersion of rhodium precursors. However, during a follow-up high-temperature thermal treatment, rhodium oxides nanoparticles suffer severe agglomeration owning to a weak rhodium-silica interaction [21]. TiO_2 with a strong interaction strengthens the stability of rhodium nanoparticles, while the low surface area leads to a poor metal dispersion [22–24]. Thus, a rational design strategy that can optimize the particle distribution and stability of supported rhodium nanoparticles is highly attractive.

Previous studies showed that supports play an essential role in the catalytic activity and products distribution for rhodium catalysts [25–28]. For example, a 2 wt% Rh/TiO_2 showed a CO conversion 8 times as high as the SiO_2 supported Rh catalyst together with an improved C2-oxygenates selectivity [27]. However, TiO_2 supported Rh catalysts without promotors still primarily produce methane with low C2-oxygenates yield [25–27]. In this sense, a variety of promotors (e.g. La, Mn, Fe, Li, etc.) have been investigated in order to improve C2-oxygenates selectivity by inhibiting the production of methane [26–31]. For instance, adding small amount of Fe and/or Mn into a Rh/TiO_2 catalyst was proven to largely promote the production of ethanol and acetaldehyde at the expense of CH_4 selectivity [27, 28]. Owning to the significant promotion effect, the structure and function of Mn in Rh-based catalysts have been widely studied, and MnO in close contact with Rh nanoparticles is in general considered to be the active phase of the promoter [32–36]. The promotion functions of Mn consist of (i) increasing Rh dispersion; [15, 35] (ii) stabilizing partially oxidized Rh sites for CO insertion; [33, 37] and (iii) generating interfacial sites between Rh and MnO to accelerate CO dissociation [32, 36]. Hence, a correlation between MnO distribution and C2-oxygenates selectivity would exist in the Mn-promoted Rh catalyst. Normally, co-impregnation is the most popular strategy to prepare bimetallic catalysts [26]. However, the random deposition of Mn on the catalyst surface largely hinders the evaluation of distribution-promotion relations. In this sense, stepwise impregnation approach would be an alternative to accurately design multicomponent catalyst [32, 38].

In this study, to further investigate the relationship between the distribution and promotion functions of Mn in multicomponent-promoted Rh catalysts, a series of Rh-based catalysts were prepared by supporting Rh, Mn, and Li on a high-surface-area SiO_2 support with a thin layer of TiO_2 on the silica surface. The addition of Li in this study is attributed to the fact that Li was reported to some extent to inhibit methane formation and boost C2-oxygenates selectivity [39–41]. Catalyst synthesis is composed of several steps: (i) depositing a thin layer of TiO_2 on SiO_2; (ii) introducing Mn on Rh or other way around by stepwise incipient-wetness-impregnation (IWI) on the prepared TiO_2/SiO_2; (iii) impregnating Li by a further IWI. With this strategy, we demonstrate that the thin TiO_2 layer on the surface of SiO_2 plays a crucial role in stabilizing Rh nanoparticles in right dispersion. Furthermore, Rh on MnO is more efficient in promoting the hydrogenation of acetaldehyde to ethanol compared to its counterpart with MnO on Rh. Finally, the catalytic performance of the multicomponent Rh-based catalyst also depends on Rh particle size, and catalyst with a larger Rh nanoparticle size exhibits a higher activity and C2-oxygenates selectivity, but lower methane selectivity than its counterpart with smaller Rh nanoparticles. This approach will provide new insight for the rational design of highly active and selective Rh based catalysts for C2-oxygenates production.

2 Experimental Section

2.1 Materials

Dihydroxybis(ammonium lactato)titanium(IV) ($C_6H_{18}N_2O_8Ti$, 50% w/w aq. soln) was purchased from Alfa Aesar, rhodium(III) chloride hydrate ($RhCl_3{\cdot}xH_2O$, 40 wt% Rh) was purchased from Tanaka Kikinzoku Kogyo KK, manganese(II) chloride tetrahydrate ($MnCl_2{\cdot}4H_2O$, > 99.9%); lithium chloride monohydrate ($LiCl{\cdot}H_2O$, > 99.9%) and citric acid ($C_6H_8O_7$, > 98%) were purchased from Wako Pure

Chemical Industries, Ltd. All the chemicals were used without further purification. SiO_2 with an average pore size of 6 nm was provided by Fuji Silysia Chemical, Ltd.

2.2 Catalyst Synthesis

SiO_2 support was washed with nitric acid (10 wt%) overnight, followed by washing with deionized water until the pH reaches neutral. The powder was further dried in air at 383 K overnight, followed by calcination at 673 K for 4.5 h, with a ramping rate of 4 K/min.

Ti/SiO_2-*673* was prepared by IWI of 2 g SiO_2 with a aqueous mixture of 0.098 g $C_6H_{18}N_2O_8Ti$ and 1.414 g deionized water. The impregnated sample was kept in a desiccator at room temperature for 0.5 h, dried in an oven at 383 K for 3 h, and further heated to 673 K for 4.5 h in stagnant air.

2 g Ti/SiO_2 was impregnated with a aqueous mixture of 0.2188 g $RhCl_3{\cdot}xH_2O$, 0.1064 g $C_6H_8O_7$ and 1.164 g deionized water, dried at 383 K for 3 h, and calcined at 673 K for 4.5 h in stagnant air. The sample was denoted as Rh/Ti/SiO_2-*673*.

2 g Rh/Ti/SiO_2-*673* was impregnated with a aqueous mixture of 0.0865 g $MnCl_2{\cdot}4H_2O$, 0.112 g $C_6H_8O_7$ and 1.22 g deionized water, dried at 383 K for 3 h, and calcined at 673 K for 4.5 h in stagnant air. The sample was denoted as Mn/Rh/Ti/SiO_2-*673*.

2 g Mn/Rh/Ti/SiO_2-*673* was impregnated with a aqueous mixture of 0.010 g $LiCl{\cdot}H_2O$, 0.112 g $C_6H_8O_7$ and 1.22 g deionized water, dried at 383 K for 3 h, and calcined at 673 K for 4.5 h in stagnant air. The sample was denoted as Li/Mn/Rh/Ti/SiO_2-*673*, and abbreviated as CAT-I-*673*.

For the preparation of CAT-I-*773 (*Li/Mn/Rh/Ti/SiO_2-*773)*, all the steps were the same as that of CAT-I-*673*, except changing the calcination temperature of section '*2.22*' to 773 K.

For the preparation of CAT-II-*673 (*Li/Rh/Mn/Ti/SiO_2-*673)*, all the preparation conditions were the same as that of CAT-I-*673*, except that the impregnation sequence of Mn and Rh was opposite.

2.3 Characterization

The N_2 adsorption–desorption measurements were performed by using Micromeritics Tristar 3020 apparatus at 77 K. Prior to measurement, samples were degassed under vacuum at 423 K overnight. The Rh, Mn, and Li contents in the samples were measured by atomic adsorption spectroscopy (AAS) (Analyst 200, Perkin Elmer, USA).

Transmission electron microscopy (TEM) characterization was performed by using a Talos F200X microscope (FEI, Hillsboro, OR, USA) at an acceleration voltage of 200 kV.

X-ray diffraction (XRD) patterns were recorded on a Bruker D8 Advance X-ray diffractometer equipped with a Co $K\alpha$ radiation ($\lambda = 0.179026$ nm) in the 2θ region between 20° and 80°.

Temperature-programmed reduction in hydrogen ($TPR(H_2)$) was performed in a homemade fixed bed reactor system connected to a thermal conductivity detector (TCD) to monitor the consumption of hydrogen by the as-prepared catalysts. 50 mg of fresh catalyst was heated in a flow of 10 vol % H_2/Ar (30 ml/min) from ambient temperature to 700 K at a heating rate of 5 K/min.

In-situ DRIFTS of CO adsorption was performed in a Nicolet 6700 FT-IR (Thermo Scientific) equipped with a MCD/A detector. Samples were reduced by pure H_2 flow (20 cm^3/min) at 673 K for 15 min (5 K/min). Afterwards, the cell was evacuated with He at 673 K for 20 min to remove the adsorbed H_2 molecules on the catalyst surface, followed by cooling down to 308 K under He flow (20 cm^3/min). Then 1.5 vol% CO/He (20 cm^3/min) was fed to the cell for 20 min at 308 K. Subsequently, the catalysts were flushed in He (20 cm^3/min) for 20 min. Then the IR spectra were consecutively collected at different temperatures.

2.4 Catalyst Performance

Catalyst activity tests were performed in a six-flow fixed-bed microreactor (FBM) setup as previously described [42]. Prior to the operation, 100 mg fresh catalysts (50–100 μm) mixed with SiC were activated in situ by H_2 at 593 K for 2.5 h at atmospheric pressure, followed by cooling to 473 K under H_2. As the pressure was increased to 20 bar, feed composition was changed from H_2 to a mixture of H_2, CO and N_2 in total of 40 ml/min (molar ratio: H_2:CO:N_2 = 10:5:6) at 473 K. Then the reactor was heated to different reaction temperature with a heating rate of 2 K/min. All the reactions were run for 8 h, after which a steady state was achieved, and products were analyzed after 8 h time-on-stream (TOS) using an online GC (Trace GC-Interscience). Methanol, acetaldehyde, ethanol and C2–C3 hydrocarbon were detected by a flame ionization detector (FID), while H_2, CO, CO_2, and CH_4 were analyzed by a thermal conductivity detector (TCD). Products selectivity was calculated from each component detected via online GC using N_2 as an internal standard, from the total amount of CO converted.

3 Results and Discussion

3.1 Characterization of the As-Synthesized Catalysts

The textural properties of SiO_2 support and as-synthesized supported Rh catalysts were determined by N_2 sorption method (Fig. S1). The SiO_2 support exhibits a mesoporous structure, as proved by the type IV curve with type H_2 hysteresis that closes at $P/P_0 \approx 0.4$ in the N_2 adsorption–desorption isotherms, demonstrating the presence of ink-bottle shape of pores. After stepwise impregnation and calcination treatments, the shape of isotherms did not change, while the BET surface area (*S*) and pore volume (*V*) of catalysts slightly decreased compared to the original SiO_2 (Table S1). The small differences can be probably due to the blockage of pores by nanoparticles and/or collapse of pore structure during high temperature treatment. Elemental analysis confirms a similar content of rhodium, manganese, and lithium in these as-synthesized supported rhodium catalysts (Table S1).

Freshly prepared supported rhodium catalysts were further studied by transmission electron microscopy technique (TEM) combined with energy-dispersive X-ray spectroscopy (EDX). After the deposition of Ti precursor followed by a thermal treatment, uniformly dispersed TiO_2 on SiO_2 surface is observed (Fig. S2). Since TiO_2 is known to contain a large number of surface hydroxyl groups, these hydroxyl groups can provide anchors for rhodium precursors, stabilize rhodium nanoparticles, and impede their growth and agglomeration during the subsequent thermal treatment [26]. Indeed, the presence of a thin layer of TiO_2 on the surface of SiO_2 to a large extent improve the dispersion of Rh_2O_3 nanoparticles compared to that in a similar Rh/SiO_2 catalyst (Fig. S3a, b). In the multicomponent promoted Rh catalysts, the Rh particle size and distribution largely depend on the calcination temperature. CAT-I-*673* and CAT-II-*673* show a homogenous distribution of Rh_2O_3 nanoparticles with an average Rh nanoparticle size around ~ 1.5 nm (Fig. 1a, b). Further raising the calcination temperature to 773 K leads to an increase of Rh nanoparticle size to 2.8 nm, with some large clusters consisting of small Rh_2O_3 crystals (Fig. 1c). EDX analysis displays overlapping signals of Rh and Mn on TiO_2/SiO_2, and a close interaction between Rh and Mn can be expected. The small size of rhodium oxide nanoparticles is

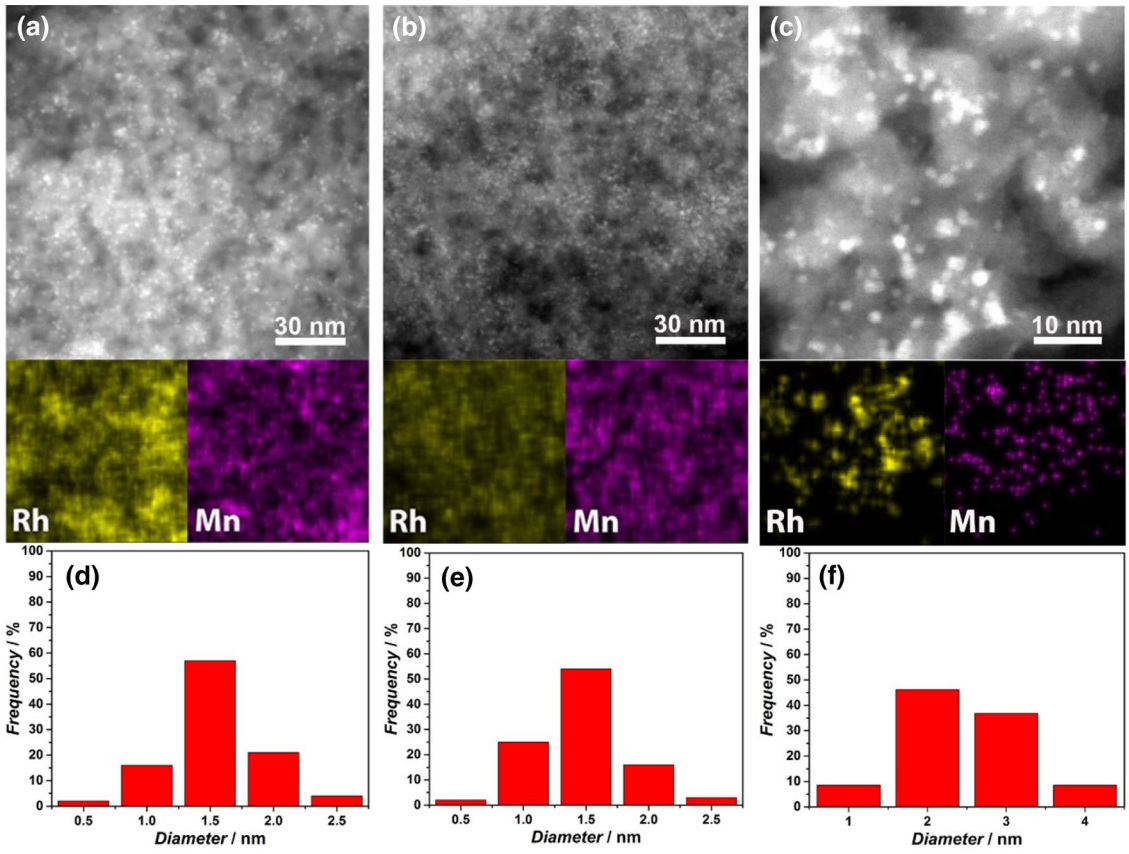

Fig. 1 Dark field TEM images and Rh particle size distribution of **a**, **d**; CAT-I-*673*; **b**, **e** CAT-II-*673*; and **c**, **f** CAT-I-*773* catalysts, with element distribution of Rh and Mn

further supported by the powder XRD analysis. As shown in Fig. 2a, the characteristic diffraction peaks for Rh_2O_3 (104) and (110) planes at 2θ value of ~ 38 and ~ 41° are broad and small, confirming the high dispersion. At the same time, the absence of diffraction peaks for Mn and Li species can be ascribed to their highly dispersed states and low loadings in these samples.

The reducibility of Rh species in all these as-synthesized samples was studied by temperature-programmed reduction in H_2 [TPR(H_2)]. As present in Fig. 2b, only one reduction peak is observed in all these Rh-based catalysts, attributed to the reduction of rhodium oxide to its metallic phase [43, 44]. The reduction profiles of Rh depend on the impregnation sequence of Mn and Rh precursors and the calcination temperature. CAT-I-*673* and CAT-II-*673* exhibit a sharp reduction peak, suggesting that supported Rh_2O_3 nanoparticles in each sample have similar properties, supporting the narrow Rh particle size distribution. CAT-I-*673* exhibits a higher temperature for Rh reduction than that of CAT-II-*673*, indicative for a stronger interaction between Mn and Rh in CAT-I-*673*. Moreover, further raising calcination temperature to 773 K shifts the reduction peak to a high temperature, and leads to a much broader peak than that in CAT-I-*673*, supporting the heterogeneity of Rh particle size distribution.

FTIR spectroscopy of adsorbed CO has been widely employed to study the nature of surface sites in most transition metal based catalysts due to the sensitivity of the CO stretching frequency to the electronic state of the adsorption sites [11]. Figure 3 together with Fig. S4 show the results obtained applying this CO adsorption technique on all these as-synthesized catalysts. No obvious CO adsorption bands can be observed from SiO_2 support itself (Fig. S4a). The rhodium-based catalysts exhibit similar features, as shown in Figs. 3a–d and S4b–d. Two regions at 2150–1950 cm^{-1} and 1950–1650 cm^{-1} are clearly observed in the spectra of pre-adsorbed CO. In the region of 2150–1950 cm^{-1}, the band centered at ~ 2070 cm^{-1} is attributed to the linearly adsorbed CO on Rh^0 sites [CO(l)], and the doublet at ~ 2102 cm^{-1} and ~ 2038 cm^{-1} can be assigned to the symmetric and asymmetric stretching vibration of a gem-dicarbonyl $Rh^+(CO)_2$, [CO(gdc)] [45]. No bands around 2145 cm^{-1} and 2135 cm^{-1} are detected, indicative of the absence of Rh^{3+} and Rh^{2+} species in these samples [45].

The feature of these CO adsorption bands varies with an increase of temperature, especially in the range of 2150–1950 cm^{-1}. Taking the '*−773*' samples for instance, the band of linearly adsorbed CO gradually becomes weaker together with an obvious shift of the intensity maximum to a lower wavenumber as the temperature increases, owning to a weaker dipolar coupling between CO molecules at a lower CO surface coverage. Although the intensity of gem-dicarbonyl $Rh^+(CO)_2$ signals decreases with temperature as well, the bands stay at the identical position. The development of these dicarbonyl complex bands demonstrates that these adsorption sites are spatially isolated, since close proximity of adsorbed CO molecules is supposed to lead to dipole–dipole interaction and, therefore, a shift to lower wavenumbers as surface coverage should decrease [45]. Furthermore, the representative signals of $Rh^+(CO)_2$ gradually decrease with an increase of temperature, indicative of a weak adsorption energy of CO molecules on these rhodium sites. The feature of these CO adsorption bands varies with the composition in the catalysts as well. Rh–Ti/SiO_2-*773* exhibits a higher fraction of CO(gdc) species than that of Mn–Rh–Ti/SiO_2-*773* and CAT-I-*773*. The presence of Li in CAT-I-*773* improves the adsorption strength of the CO(gdc) species, as proven by the presence of CO adsorption band at ~ 2102 cm^{-1} at 423 K.

In the region of 1950–1650 cm^{-1}, a broad shoulder with a tail is present, suggesting the existence of several kinds of

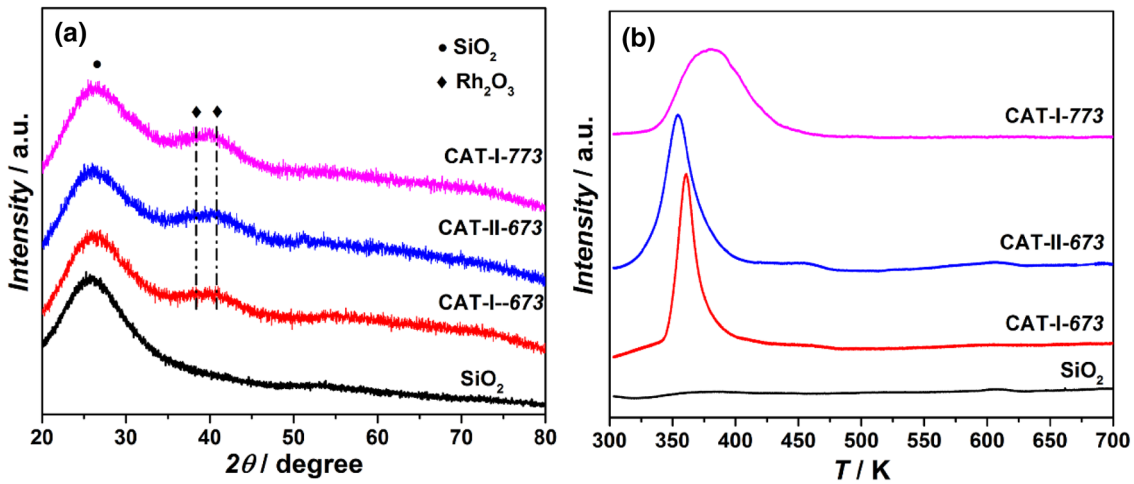

Fig. 2 **a** XRD patterns and **b** TPR(H_2) profiles of the as-synthesized supported Rh catalysts

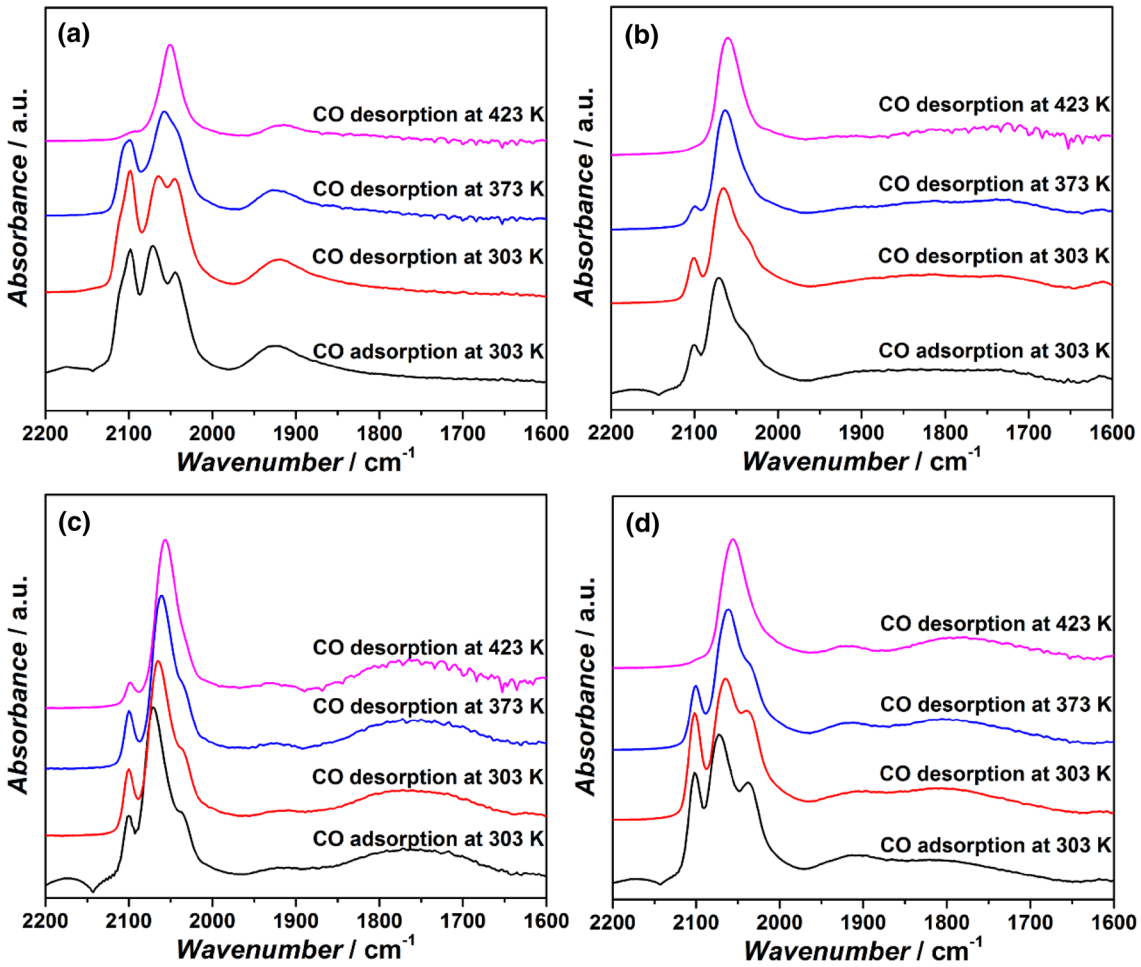

Fig. 3 DRIFT spectra of CO adsorbed on **a** Rh-Ti/SiO_2-*773*, **b** Mn-Rh-Ti/SiO_2-*773*, **c** CAT-I-*773,* and **d** CAT-I-*673* catalysts at different temperatures

CO adsorption sites at the surface of rhodium nanoparticles. Specifically, the broad bands between 1950 and 1750 cm^{-1} represent the existence of bridge bonded CO on Rh^0 [46]. The tail with a wavenumber ranging from 1750 cm^{-1} to 1650 cm^{-1} [CO(t)] is too low to be attributed to CO bridge-bonded to several Rh atoms via carbon atom alone. Similar bands at 1725 cm^{-1} and 1696 cm^{-1} were also detected by Lisitsyn et al. [21] These bridging sites have been considered as the metal/oxide interfacial sites, on which the C and O in CO molecule are bonded to metallic Rh and $Mn^{\delta+}$ cation, respectively, namely a tilted Rh–C–O–Mn species [21, 38, 47]. Such an adsorption state should weaken the C–O bond and enhance CO dissociation.

Finally, the intensity ratio between CO(l) and CO(gdc) bands varies between catalysts prepared at different temperatures. The '*−673*' samples show a similar CO(l)/CO(gdc) value but lower than that of the '*−773*' sample (Figs. 3c, d and S4d). Since the dicarbonyl Rh^+ species are predominantly formed on highly dispersed rhodium nanoparticles, the relatively higher intensity of the dicarbonyl bands in the '*−673*' samples further supports the smaller rhodium size than that in the '*−773*' sample [19, 29]. In contrast, the intensity ratio between CO(l) and CO(t) for the '*−673*' samples is higher than that in the '*−773*' sample, indicative of a higher fraction of tilted Rh–C–O–Mn species on the '*−773*' surface.

3.2 Roles of Rh Particle Size and Promoters on Hydrogenation Activity and Products Selectivity

CO conversions over these supported Rh catalysts after 8 h time-on-stream (TOS) (after which CO conversion becomes stable) at 533 K, 20 bar, H_2/CO molar ratio of 2 are presented in Fig. 4a. The catalytic performance of these Rh-based catalysts displays different CO conversion levels. CAT-I-*773* shows a higher CO conversion (3.9%) than that of the CAT-I-*673* (2.3%) and CAT-II-*673* (1.2%). In

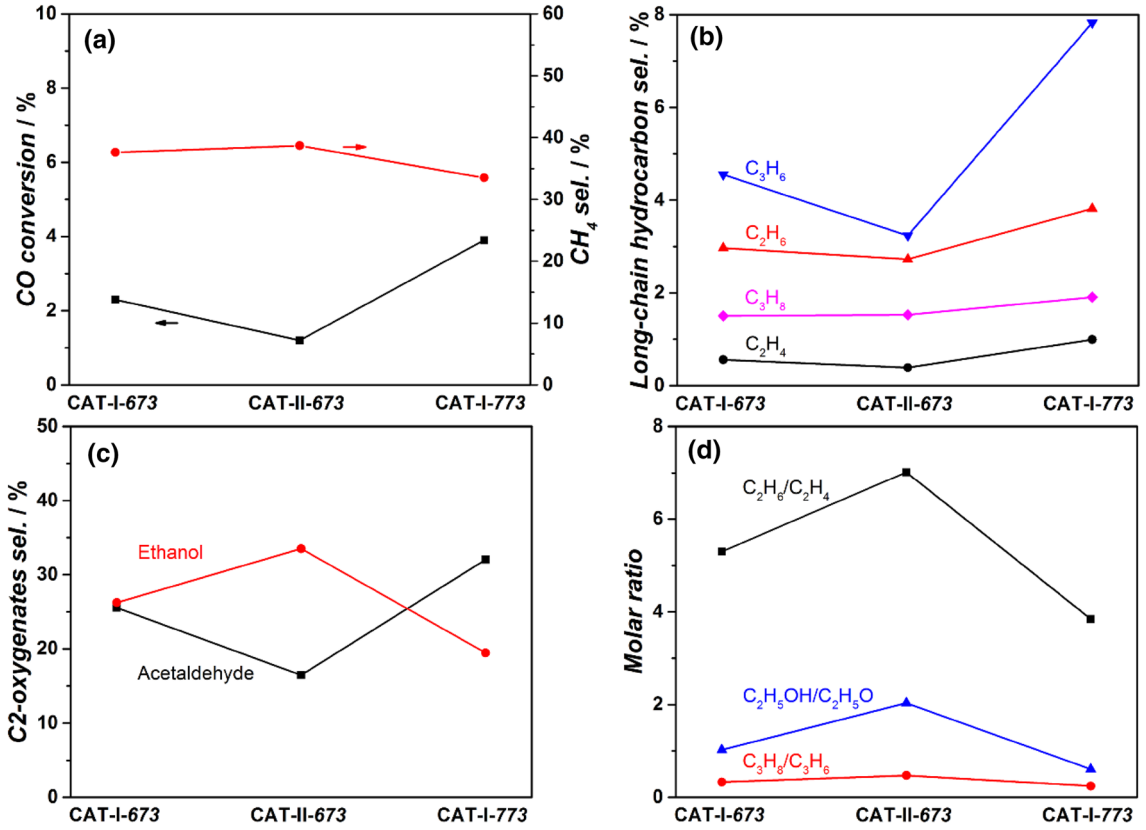

Fig. 4 **a** CO conversion and CH_4 selectivity; **b** long-chain hydrocarbon selectivity; **c** C2-oxygenates selectivity and **d** products molar ratio for CAT-I-*673*, CAT-II-*673*, and CAT-I-*773* catalysts after 8 h TOS at 533 K, 20 bar total pressure, and feed composition $H_2/CO = 2$

principle, small Rh nanoparticles in CAT-I-*673* exhibit a much stronger interaction with the thin TiO_2 layer on SiO_2 support compared to the large ones in CAT-I-*773* [11, 20]. The strong Rh-TiO_2 interaction generates a large number of electron-deficient Rh atoms on the surface, which results in poor electron back-donation to the unoccupied $2\pi^*$ antibonding orbital of CO, thereby impeding CO dissociation and further hydrogenation. Moreover, MnO promoter has also been reported to improve the hydrogenation activity of supported Rh catalysts [32, 48]. For instance, Wang et al. found that adding 1.1 wt% Mn to a carbon nanotubes(CNTs) supported 4.5 wt% Rh catalyst led to a CO conversion two times as high as that of 4.5 wt% Rh/CNTs [48]. Schwartz et al. also reported a similar trend after introducing 0.5 wt% Mn into 1 wt% Rh/TiO_2 [26]. In general, hydrogenation of CO to formyl species intermediate is considered as the rate limiting step on Rh-based catalyst [30, 49]. The introduction of Mn species can generate Rh–MnO interfacial sites on the surface of Rh nanoparticles. CO molecules adsorb on these sites in a tilted Rh–C–O–Mn mode, which shows a high CO dissociation activity [38, 47]. Obviously, the larger Rh nanoparticle size and the higher fraction of tilted Rh–C–O–Mn species in CAT-I-*773* than the '*−673*' samples lead to a higher hydrogenation activity.

The products distributions for all these Rh based catalysts after 8 h are included in Fig. 4a–d. Negligible CO_2 and methanol was detected in all these as-synthesized Rh based catalysts under this experimental condition. Previous studies demonstrated that both metallic and partially positive Rh sites are necessary in the production of C2-oxygenates [15, 50]. Metallic Rh (Rh^0) was considered for C–O bonds dissociation to produce '$–CH_x$' species, and positive Rh ($Rh^{\delta+}$) was responsible for CO insertion [15]. In this sense, parameters that can adjust the molar ratio of $Rh^0/Rh^{\delta+}$ in Rh nanoparticles are supposed to influence products distribution [27, 29]. Haider et al. proved that Rh/SiO_2 with a weak Rh-support interaction mainly produces hydrocarbons, while more C2-oxygenates were detected on Rh/TiO_2 with a strong-metal-support-interaction (SMSI) at the expense of hydrocarbons [27]. The improvement in C2-oxygenates production on TiO_2 was attributed to its stronger interaction with Rh nanoparticles, which creates more $Rh^{\delta+}$ sites. Similarly in the current work, the thin TiO_2 layer on SiO_2 support interacts strongly with Rh nanoparticles, and generates numerous partially positive Rh sites necessary for CO insertion in C2-oxygenates production. Besides, the particle size of supported Rh nanoparticles can also influence the molar ratio of $Rh^0/Rh^{\delta+}$ at the surface of Rh nanoparticles.

In general, as Rh nanoparticles become smaller, the electron-interaction between the support and Rh nanoparticles becomes stronger, and more electrons from Rh can be withdrawn by the support; hence more $Rh^{\delta+}$ sites at the surface can be created. Indeed, the '*–673*' samples exhibit a much higher fraction of $Rh^{\delta+}$ sites than CAT-I-*773*, as confirmed in Fig. 2c. Previous study by Hironori et al. reported a volcano-like relationship between Rh nanoparticle size and C2-oxygenates selectivity with the maximum C2-oxygenates selectivity at Rh particle size of ~ 3.0 nm on a Rh/SiO_2 catalyst [51]. The CAT-I-*773* catalyst with a similar Rh particle size (~ 2.8 nm) also exhibits a higher C2-oxygenates (sum of acetaldehyde and ethanol) selectivity (~ 55%) than the '*-673*' samples with a smaller Rh particle size of ~ 1.5 nm (~ 50%). At the same time, CAT-I-*773* produces more C2-C4 hydrocarbons and less CH_4 (33% vs. 38%) compared to CAT-I-*673*, as shown in Fig. 4a, b. Indeed, large nanoparticles are known to contain more terrace sites for carbon chain growth towards long chain hydrocarbons instead of methane [52].

Beside the effects of the support and Rh particle size on products selectivity, the presence of Li and Mn in supported Rh catalysts is also of great importance for the production of C2-oxygenates in this study. Egbebi et al. and Schwartz et al. indicated that a small amount of Li (~ 0.1 wt%) significantly improved the products selectivity towards C2-oxygenates of 1 wt% Rh/TiO_2 at the expense of CH_4 production [25, 26]. The presence of Li was stated to improve the stability of the '$–CH_x$' intermediate species on the surface of Rh, making the insertion of adsorbed CO species into '$–CH_x$' to produce C2-oxygenates more competitive than the direct hydrogenation of '$–CH_x$' into methane [25, 40]. Moreover, Liu et al. reported that the addition of Mn into 3 wt% Rh/CNTs significantly promoted the production of C2-oxygenates, and C2-oxygenates selectivity seemed to increase with the loadings of Mn in the catalyst [32]. A similar phenomenon was as well observed by Schwartz et al. after introducing 0.5 wt% Mn into a 1 wt% Rh/TiO_2 catalyst [26]. Manganese species in oxidation states are well-known to act as electron acceptors and withdraw electrons from Rh to create partially positive Rh sites, necessary for CO insertion in C2-oxygenates production [32, 34]. At the same time, the tilt-adsorbed CO species at the Rh–MnO interfacial sites was reported by Wang et al. to be the precursor for the formation of oxygenates [53]. Interestingly, although CAT-I-*673* and

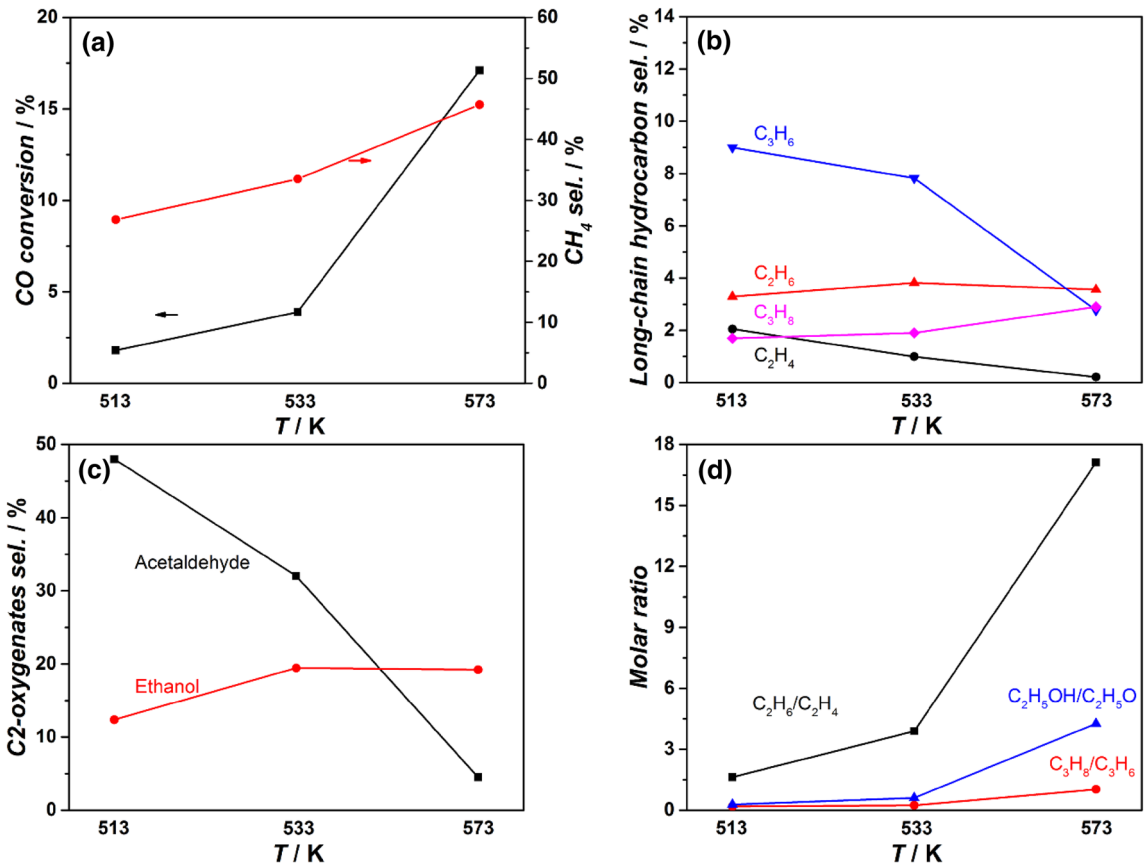

Fig. 5 **a** CO conversion and CH_4 selectivity; **b** long-chain hydrocarbon selectivity; **c** C2-oxygenates selectivity and **d** products molar ratio for CAT-I-*773* catalyst at different temperatures, 20 bar total pressure, and feed composition $H_2/CO = 2$

CAT-II-*673* show similar C2-oxygenates (sum of acetaldehyde and ethanol) selectivity, CAT-II-*673* exhibits a higher ethanol selectivity (33%) than CAT-I-*673* (26%), indicative of a higher hydrogenation capability of CAT-II-*673* with MnO underneath Rh nanoparticles, as shown in Fig. 4c, d. Indeed, H_2-TPR profile of CAT-II-*673* indicates that a lower reduction temperature is needed compared to that of CAT-I-*673*, suggestive of a relatively weaker interaction between Rh and manganese oxide and/or TiO_2 in CAT-II-*673*. The higher hydrogenation ability of CAT-II-*673* can be also demonstrated by higher ethane/ethylene and propane/propylene ratios, as shown in Fig. 4d.

3.3 Influence of Reaction Variables: Temperature and H_2:CO Ratio on Catalytic Performance

The effect of reaction temperature on the hydrogenation activity and products selectivity of the representative CAT-I-*773* sample is summarized in Fig. 5a–d. CO conversion increases from 1.8 to 17.1% as the reaction temperature increase from 513 to 573 K, while the selectivity to paraffins, especially methane increases from ~27 to ~46% at the expense of total olefins and C2-oxygenates selectivity, which decreases from 60 to 24%. These results indicate a dominant hydrogenation of '–CH_x' species at high temperature and the activation energy for methane formation is higher than that for C2-oxygenates synthesis [54]. The preferable hydrogenation reaction at high temperature is further proved by an increase of paraffin/olefin and/or ethanol/acetaldehyde ratio.

Figure 6 summarizes the influence of H_2:CO ratio ranging from 1 to 3 on the hydrogenation activity and products selectivity over CAT-I-*773*. As shown in Fig. 6a, c, despite that the CO conversion increases from 1.3 to 4.8% with H_2 concentration in the feed, the selectivity to methane also increased from 27 to 44% at the expense of acetaldehyde, which decreases from 46 to 12%. Indeed, a high concentration of hydrogen on the surface on one hand promotes the termination step of '–CH_x' species, leading to high CH_4 production; on the other hand enhances the hydrogenation steps of unsaturated C=C and C=O bonds, resulting in high product selectivity to paraffin and ethanol at the expense of olefins and acetaldehyde, as confirmed in Fig. 6b–d. These

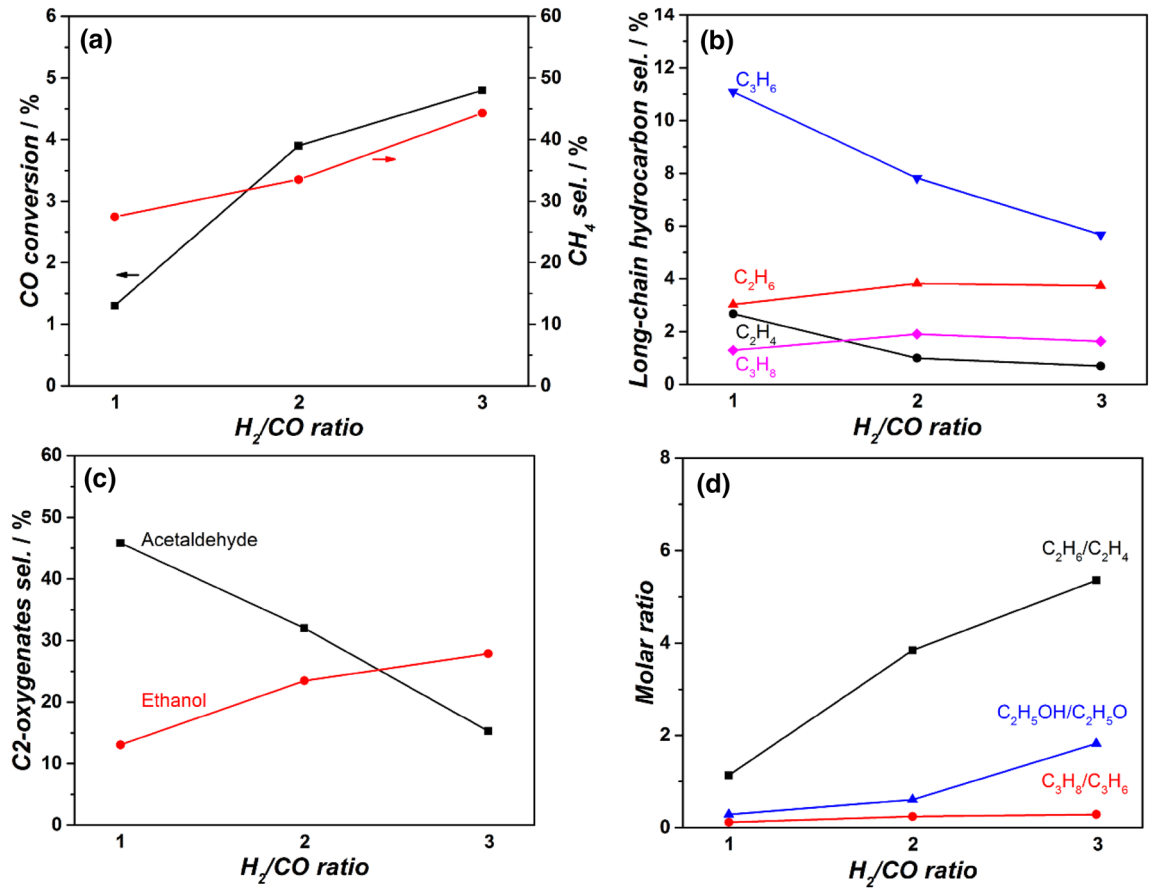

Fig. 6 **a** CO conversion and CH_4 selectivity; **b** long-chain hydrocarbon selectivity; **c** C2-oxygenates selectivity and **d** products molar ratio for CAT-I-*773* catalyst at 533 K, 20 bar total pressure, and different feed compositions

results suggest that to target C2-oxygenates synthesis, reaction is preferred to be operated at a low temperature with a low H_2/CO molar ratio in the feed.

4 Conclusions

In this work, Mn and Li promoted Rh catalysts supported on SiO_2 with a thin TiO_2 layer were prepared by stepwise incipient wetness impregnation method. The thin TiO_2 layer on the surface of SiO_2 was crucial to stabilize those small Rh nanoparticles and hamper their agglomeration. The reducibility of Rh on these catalysts is dependent on both Rh particle size and the location of manganese oxide. Large Rh nanoparticles beneath MnO can be reduced at a higher temperature than small Rh nanoparticles on MnO. Large Rh particles show a higher CO conversion and higher products selectivity towards long chain hydrocarbons and C2-oxygenates, but a lower methane selectivity compared to a similar catalyst with smaller Rh particles. The high catalytic performance to C2-oxygenates with large Rh nanoparticles is ascribed to both the promotion effect of Mn and Li, and a proper molar ratio between metallic Rh (Rh^0) sites and partially positive Rh ($Rh^{\delta+}$) sites on the surface of Rh nanoparticles. Moreover, the catalyst with MnO underneath the Rh nanoparticles is more efficient in promoting hydrogenation of acetaldehyde to ethanol than a similar catalyst with MnO on Rh nanoparticles. In order to reach high C2-oxygenates selectivity, reaction is recommended to be performed at a low temperature together with a low H_2/CO ratio in the feed.

References

1. Rostrup-Nielsen JR (2005) Making fuels from biomass. Science 308:1421–1422
2. Schmidt LD, Dauenhauer PJ (2007) Hybrid routes to biofuels. Nature 447:914
3. Song C (2006) Global challenges and strategies for control, conversion and utilization of CO_2 for sustainable development involving energy, catalysis, adsorption and chemical processing. Catal Today 115:2–32
4. Ahmed A, Lewis RS (2007) Fermentation of biomass-generated synthesis gas: effects of nitric oxide. Biotechnol Bioeng 97:1080–1086
5. Farrell AE, Plevin RJ, Turner BT, Jones AD, O'Hare M, Kammen DM (2006) Ethanol can contribute to energy and environmental goals. Science 311:506–508
6. Spivey JJ, Egbebi A (2007) Heterogeneous catalytic synthesis of ethanol from biomass-derived syngas. Chem Soc Rev 36:1514–1528
7. Subramani V, Gangwal SK (2008) A review of recent literature to search for an efficient catalytic process for the conversion of syngas to ethanol. Energy Fuels 22:814–839
8. Zaman S, Smith KJ (2012) A review of molybdenum catalysts for synthesis gas conversion to alcohols: catalysts, mechanisms and kinetics. Catal Rev 54:41–132
9. Vannice MA (1975) The catalytic synthesis of hydrocarbons from H2CO mixtures over the group VIII metals: I. The specific activities and product distributions of supported metals. J Catal 37:449–461
10. Poutsma ML, Elek LF, Ibarbia PA, Risch AP, Rabo JA (1978) Selective formation of methanol from synthesis gas over palladium catalysts. J Catal 52:157–168
11. Sun X, Sartipi S, Kapteijn F, Gascon J (2016) Effect of pretreatment atmosphere on the activity and selectivity of Co/mesoHZSM-5 for Fischer-Tropsch synthesis. New J Chem 40:4167–4177
12. Sun X, Suarez AIO, Meijerink M, van Deelen T, Ould-Chikh S, Zečević J, de Jong KP, Kapteijn F, Gascon J (2017) Manufacture of highly loaded silica-supported cobalt Fischer-Tropsch catalysts from a metal organic framework. Nat Commun 8:1680
13. Wezendonk TA, Sun X, Dugulan AI, van Hoof AJF, Hensen EJM, Kapteijn F, Gascon J (2018) Controlled formation of iron carbides and their performance in Fischer-Tropsch synthesis. J Catal 362:106–117
14. Cheng Q, Tian Y, Lyu S, Zhao N, Ma K, Ding T, Jiang Z, Wang L, Zhang J, Zheng L, Gao F, Dong L, Tsubaki N, Li X (2018) Confined small-sized cobalt catalysts stimulate carbon-chain growth reversely by modifying ASF law of Fischer-Tropsch synthesis. Nat Commun 9:3250
15. Watson PR, Somorjai GA (1981) The hydrogenation of carbon monoxide over rhodium oxide surfaces. J Catal 72:347–363
16. Bhasin MM, Bartley WJ, Ellgen PC, Wilson TP (1978) Synthesis gas conversion over supported rhodium and rhodium-iron catalysts. J Catal 54:120–128
17. Burch R, Petch MI (1992) Investigation of the synthesis of oxygenates from carbon monoxide/hydrogen mixtures on supported rhodium catalysts. Appl Catal A 88:39–60
18. Erdöhelyi A, Solymosi F (1983) Effects of the support on the adsorption and dissociation of CO and on the reactivity of surface carbon on Rh catalysts. J Catal 84:446–460
19. Basu P, Panayotov D, Yates JT (1988) Rhodium-carbon monoxide surface chemistry: the involvement of surface hydroxyl groups on alumina and silica supports. J Am Chem Soc 110:2074–2081
20. Ojeda M, Rojas S, Boutonnet M, Pérez-Alonso FJ, García-García FJ, Fierro JLG (2004) Synthesis of Rh nano-particles by the microemulsion technology: particle size effect on the $CO + H_2$ reaction. Appl Catal A 274:33–41
21. Lisitsyn AS, Stevenson SA, Knözinger H (1990) Carbon monoxide hydrogenation on supported Rh-Mn catalysts. J Mol Catal 63:201–211
22. Rives-Arnau V, Munuera G (1980) Effect of strong metal-support interactions on the catalytic reduction of NO by TiO_2-supported rhodium. Appl Surf Sci 6:122–137
23. Gajardo P, Gleason EF, Katzer JR, Sleight AW (1981) Preparation and characterization of highly dispersed rhodium on Al_2O_3, TiO_2, ZrO_2, and CeO_2. In: Seiyama T, Tanabe K (eds) Studies in surface science and catalysis. Elsevier, Amsterdam, pp 1462–1463
24. Vis JC, Van't Buk HFJ, Huizinga T, Van Grondelle J, Prins R (1984) Reduction and oxidation of Rh/Al_2O_3 and Rh/TiO_2 catalysts as studied by temperature-programmed reduction and oxidation. J Mol Catal 25:367–378

25. Egbebi A, Schwartz V, Overbury SH, Spivey JJ (2010) Effect of Li promoter on titania-supported Rh catalyst for ethanol formation from CO hydrogenation. Catal Today 149:91–97
26. Schwartz V, Campos A, Egbebi A, Spivey JJ, Overbury SH (2011) EXAFS and FT-IR characterization of Mn and Li promoted titania-supported Rh catalysts for CO hydrogenation. ACS Catal 1:1298–1306
27. Haider MA, Gogate MR, Davis RJ (2009) Fe-promotion of supported Rh catalysts for direct conversion of syngas to ethanol. J Catal 261:9–16
28. Palomino RM, Magee JW, Llorca J, Senanayake SD, White MG (2015) The effect of Fe–Rh alloying on CO hydrogenation to C2+ oxygenates. J Catal 329:87–94
29. Gao J, Mo X, Chien AC-Y, Torres W, Goodwin JG (2009) CO hydrogenation on lanthana and vanadia doubly promoted Rh/SiO_2 catalysts. J Catal 262:119–126
30. Yang N, Yoo JS, Schumann J, Bothra P, Singh JA, Valle E, Abild-Pedersen F, Nørskov JK, Bent SF (2017) Rh-MnO interface sites formed by atomic layer deposition promote syngas conversion to higher oxygenates. ACS Catal 7:5746–5757
31. Bezemer GL, Radstake PB, Falke U, Oosterbeek H, Kuipers HPCE, van Dillen AJ, de Jong KP (2006) Investigation of promoter effects of manganese oxide on carbon nanofiber-supported cobalt catalysts for Fischer-Tropsch synthesis. J Catal 237:152–161
32. Liu J, Guo Z, Childers D, Schweitzer N, Marshall CL, Klie RF, Miller JT, Meyer RJ (2014) Correlating the degree of metal–promoter interaction to ethanol selectivity over MnRh/CNTs CO hydrogenation catalysts. J Catal 313:149–158
33. Mei D, Rousseau R, Kathmann SM, Glezakou V-A, Engelhard MH, Jiang W, Wang C, Gerber MA, White JF, Stevens DJ (2010) Ethanol synthesis from syngas over Rh-based/SiO_2 catalysts: a combined experimental and theoretical modeling study. J Catal 271:325–342
34. van den Berg FGA, Glezer JHE, Sachtler WMH (1985) The role of promoters in COH_2 reactions: effects of MnO and MoO_2 in silica-supported rhodium catalysts. J Catal 93:340–352
35. Wang Y, Song Z, Ma D, Luo H, Liang D, Bao X (1999) Characterization of Rh-based catalysts with EPR, TPR, IR and XPS. J Mol Catal A 149:51–61
36. Wilson TP, Kasai PH, Ellgen PC (1981) The state of manganese promoter in rhodium-silica gel catalysts. J Catal 69:193–201
37. Ojeda M, Granados ML, Rojas S, Terreros P, García-García FJ, Fierro JLG (2004) Manganese-promoted Rh/Al_2O_3 for C2-oxygenates synthesis from syngas: effect of manganese loading. Appl Catal A 261:47–55
38. Brundage MA, Balakos MW, Chuang SSC (1998) LHHW and PSSA kinetic analysis of rates and adsorbate coverages in $CO/H_2/C_2H_4$ reactions on Mn–Rh/SiO_2. J Catal 173:122–133
39. Kusama H, Okabe K, Sayama K, Arakawa H (1996) CO_2 hydrogenation to ethanol over promoted Rh/SiO_2 catalysts. Catal Today 28:261–266
40. Chuang SC, Goodwin JG, Wender I (1985) The effect of alkali promotion on CO hydrogenation over $RhTiO_2$. J Catal 95:435–446
41. Tien-Thao N, Hassan Zahedi-Niaki M, Alamdari H, Kaliaguine S (2007) Effect of alkali additives over nanocrystalline Co–Cu-based perovskites as catalysts for higher-alcohol synthesis. J Catal 245:348–357
42. Hakeem AA, Vásquez RS, Rajendran J, Li M, Berger RJ, Delgado JJ, Kapteijn F, Makkee M (2014) The role of rhodium in the mechanism of the water–gas shift over zirconia supported iron oxide. J Catal 313:34–45
43. Wong C, McCabe RW (1987) Effects of oxidation/reduction treatments on the morphology of silica-supported rhodium catalysts. J Catal 107:535–547
44. Lopez L, Velasco J, Montes V, Marinas A, Cabrera S, Boutonnet M, Järås S (2015) Synthesis of ethanol from syngas over Rh/MCM-41 catalyst: effect of water on product selectivity. Catalysts 5:1737
45. Trautmann S, Baerns M (1994) Infrared spectroscopic studies of CO adsorption on rhodium supported by SiO_2, Al_2O_3, and TiO_2. J Catal 150:335–344
46. Fisher IA, Bell AT (1996) A comparative study of CO and CO_2 hydrogenation over Rh/SiO_2. J Catal 162:54–65
47. Trevino H, Lei GD, Sachtler WMH (1995) CO hydrogenation to higher oxygenates over promoted rhodium: nature of the metal-promoter interaction in Rhmn/NaY. J Catal 154:245–252
48. Wang S-R, Guo W-W, Wang H-X, Zhu L-J, Qiu K-Z (2014) Influence of Mn promotion on CO hydrogenation over Rh/CNTs catalyst. Catal Lett 144:1305–1312
49. Choi Y, Liu P (2009) Mechanism of ethanol synthesis from syngas on Rh(111). J Am Chem Soc 131:13054–13061
50. Chuang SSC, Pien SI (1992) Infrared study of the CO insertion reaction on reduced, oxidized, and sulfided Rh/SiO_2 catalysts. J Catal 135:618–634
51. Hironori A, Kazuhiko T, Takehiko M, Yoshihiro S (1984) Effect of metal dispersion on the activity and selectivity of Rh/SiO_2 catalyst for high pressure CO hydrogenation. Chem Lett 13:1607–1610
52. Van Santen RA (2009) Complementary structure sensitive and insensitive catalytic relationships. Acc Chem Res 42:57–66
53. Wang Y, Luo H, Liang D, Bao X (2000) Different mechanisms for the formation of acetaldehyde and ethanol on the Rh–based catalysts. J Catal 196:46–55
54. Gronchi P, Tempesti E, Mazzocchia C (1994) Metal dispersion dependent selectivities for syngas conversion to ethanol on V_2O_3 supported rhodium. Appl Catal A 120:115–126